Geomechanics and Engineering, *Vol. 31, No. 3 (2022) 329-337*
https://doi.org/10.12989/gae.2022.31.3.329

Thermal post-buckling analysis of porous functionally graded pipes with initial geometric imperfection

Jia-Qin Xu and Gui-Lin She*

College of Mechanical and Vehicle Engineering, Chongqing University, Chongqing 400044, China

(*Received April 15, 2022, Revised October 14, 2022, Accepted November 8, 2022*)

Abstract. In this paper, the thermal post-buckling characteristics of functionally graded (FG) pipes with initial geometric imperfection are studied. Considering the influence of initial geometric defects, temperature and geometric nonlinearity, Euler-Lagrange principle is used to derive the nonlinear governing equations of the FG pipes. Considering three different boundary conditions, the two-step perturbation method is used to solve the nonlinear governing equations, and the expressions of thermal post-buckling responses are also obtained. Finally, the correctness of this paper is verified by numerical analyses, and the effects of initial geometric defects, functional graded index, elastic foundation, porosity, thickness of pipe and boundary conditions on thermal post-buckling response are analyzed. It is found that, bifurcation buckling exists for the pipes without initial geometric imperfection. In contrast, there is no bifurcation buckling phenomenon for the pipes with initial geometric imperfection. Meanwhile, the elastic stiffness can significantly improve thermal post-buckling load and thermal post-buckling strength. The larger the porosity, the greater the thermal buckling load and the thermal buckling strength.

Keywords: boundary conditions; elastic foundation; initial geometric imperfection; porous functionally graded pipes; thermal post-buckling

1. Introduction

Pipes are common structures in nature and engineering, such as carbon nanotubes, liquid conveying pipes and steel pipes, etc. It is of great significance to analyze their mechanical behavior for engineering applications of circular pipes. Functionally graded (FG) materials are a new type of composite materials which are often used as thermal insulation coatings or structural components for aerospace vehicles (Golmakani *et al.* 2019). For example, Hadji *et al.* (2018) applied a new quasi-3d higher shear deformation theory for vibration of FG carbon nanotube-reinforced composite beams resting on elastic foundations. Alnujaie *et al.* (2021) discussed the forced vibration of an FG porous beam resting on viscoelastic foundations. Asiri *et al.* (2020) discussed the damped dynamic responses of FG thick beams subjected to pulse loadings. Amar *et al.* (2018) utilized a new four-unknown refined theory to analyze the bending and vibration analysis of FG micro-plate. Akba *et al.* (2021) performed the vibration analysis of FG porous beams with viscoelastic support. Ghandourah *et al.* (2021) analyzed the free vibrations of porous FG nonlocal modified couple nanobeams with the help of the modified porosity model. When the structure is under the action of thermal load, it will inevitably produce thermal stress, which may cause the instability of the structure. Therefore, it is necessary to study the stability of FG structures in thermal environment (Ding and She 2021, Ebrahimi and Farazmandnia 2018, Hadji *et al.* 2018, She 2021, She *et al.* 2021, Zhang *et al.* 2021, Zenkour and Radwan 2019, Akgöz and Civalek 2017, Attia 2020a, 2020b, Hendi *et al.* 2022, Zhao *et al.* 2022).

Many people have studied the mechanics of pipe structures. For instance, Fu *et al.* (2015) analyzed thermal post-buckling of FG pipes with simply supported ends using a new beam model. She *et al.* (2017a) performed the thermal post-buckling of FG pipes with two clamped ends. She *et al.* investigated the buckling and post-buckling (She *et al.* 2017b) of FG nano pipes with porosities. This work was then then extended to the buckling analysis of microtubes with geometrical imperfection (Lu *et al.* 2021). However, the paper (Lu *et al.* 2021) does not consider the effects of temperature loadings and elastic foundation. Babaei *et al.* (2021) discussed the thermoelastic buckling and post-buckling behavior of pipes reinforced with CNTs. Due to the limitation of production technology, the initial geometric imperfection will inevitably occur, which will undoubtedly affect the mechanical properties of the structure. Defects can affect the safety performance of structures, and many people have studied the influence of defects on the mechanical properties of structures. For instance, Dehrouyeh-Semnani (2016) studied the imperfection sensitivity of the free vibration of geometrically FG microbeams. He indicated that the initial geometric imperfection has great impact on the vibration problems. Babaei analyzed thermal post-buckling (Babaei 2021a) and free vibration behaviors (Babaei 2021b) of composite pipes reinforced with CNTs. This work was then extended to the case of free vibrations of curved pipes based on nonlocal strain gradient theory (Babaei 2021c). Babaei and Eslami analyzed the nonlinear bending (Babaei and

*Corresponding author, Professor
E-mail: sheguilin@cqu.edu.cn

ISSN: 2005-307X (Print), 2092-6219 (Online)

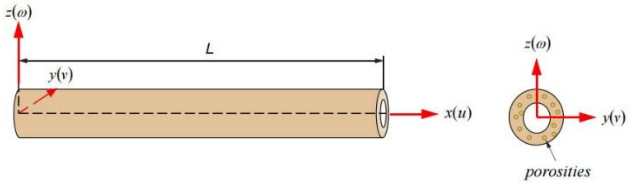

Fig. 1 Schematic diagram of an FG pipe

Eslami 2021a) and nonlinear stability (Babaei and Eslami 2021b) of clamped FG porous curved micro-tubes.

Buckling is an important issue for engineering structures, which is a structural instability failure mode of structures. Thermal buckling is a common problem for space structure design. Many scholars have extensively studied the buckling and post-buckling problems. For example, Emam (2016) analyzed the buckling and post-buckling behaviors of composite beams in hygrothermal environments. Mohamed *et al.* (2020) performed the buckling and post-buckling analysis of carbon nanotubes via the energy-equivalent model. Mohamed *et al.* (2022) dealt with nonlinear buckling of imperfect composite beams. Pinnola *et al.* (2022) conceived a consistent formulation of nonlocal elastic foundation via the Winkler and Wieghardt laws.

However, when studying the thermal post-buckling of the pipe structures, the existing papers ignore the influence of initial geometric imperfection, and in addition, there are no papers reporting the thermal post-buckling of geometrically imperfect pipe structures with one end clamped and one end simply supported. Therefore, it is necessary to study this problem. The purpose of this paper is to solve this problem.

2. Derivation of governing equations

Consider an FG pipe, its length, inner and outer radius, respectively by L, R_i, and R_o, the coordinate system is depicted in Fig. 1. The materials adopted in this paper are also shown in Table 1, and here, the subscript "*f*" is used for FG materials, the subscript "*c*" for ceramics, subscript "*m*" for metals, β for pore volume fraction, N for power law exponent. P_0, P_{-1}, P_1, P_2, and P_3 are temperature-dependent coefficients, and the valid material parameters for Young's modulus E and thermal expansion coefficient α can be described as (Fu *et al.* 2015, She *et al.* 2022)

$$\begin{aligned} E &= [E_c - E_m]\left(\frac{r-R_i}{R_0-R_i}\right)^N + E_m - \frac{\beta}{2}[E_c + E_m] \\ \alpha &= [\alpha_c - \alpha_m]\left(\frac{r-R_i}{R_0-R_i}\right)^N + \alpha_m - \frac{\beta}{2}[\alpha_c + \alpha_m] \end{aligned} \tag{1}$$

Euler-Bernoulli beam theory is adopted to describe the pipe structure, and its displacement field can be expressed as

$$u_x = u - z\frac{\partial w}{\partial x}, u_y = 0, u_z = w + w^* \tag{2}$$

In Eq. (2), u represents the axial displacement, w stands for the deflection, and w^* refers to the deflection caused by the initial geometric imperfections. We should note that Euler-Bernoulli beam theory is only valid and acceptable for the pipe structures with slenderness ratio greater than five.

Considering geometric nonlinear effect, the corresponding non-zero strain ε_{xx} can be deduced as

$$\varepsilon_{xx} = \frac{\partial u_x}{\partial x} + \frac{1}{2}\left(\frac{\partial u_z}{\partial x}\right)^2 \tag{3}$$

The influence of uniform temperature field is taken into account in this paper, so that, the axial stress σ_{xx} can be calculated as follows (Fu *et al.* 2015)

$$\sigma_{xx} = E\left(\varepsilon_{xx} - \alpha\Delta T\right) \tag{4}$$

Herein, $\Delta T\left(\Delta T = T\text{-}300\text{K}\right)$ is the elevated temperature, in which, T is the ambient temperature. It should be noted that the analysis in this paper is carried out under the special assumption of uniform temperature fields. It is worth mentioning that there are various temperature fields in engineering applications, but this paper only considers the case of uniform temperature field for convenience.

Then, integration of stress gives the expressions of stress resultant N_x and thermal loads N_T, which are as follows (Fu *et al.* 2015)

$$N_x = \int \sigma_{xx} dz,\ N_T = \int \alpha\Delta T dz \tag{5}$$

Therefore, the total energy of the system can be expressed as

$$\begin{aligned} L &= \frac{1}{2}k_1 w^2 + \frac{1}{2}k_2\left(\frac{\partial w}{\partial x}\right)^2 + \frac{1}{2}\int_A E\left(\varepsilon_x - \alpha\Delta T\right)\varepsilon_x dA \\ &= \frac{1}{2}k_1 w^2 + \frac{1}{2}k_2\left(\frac{\partial w}{\partial x}\right)^2 + \frac{1}{2}\int_A E\left\{\begin{array}{l}\left[\frac{\partial u}{\partial x} - z\frac{\partial^2 w}{\partial x^2} + \frac{1}{2}\left(\frac{\partial w}{\partial x}\right)^2 + \frac{\partial w}{\partial x}\frac{\partial w^*}{\partial x}\right]^2 \\ -\alpha\Delta T\left[\frac{\partial u}{\partial x} - z\frac{\partial^2 w}{\partial x^2} + \frac{1}{2}\left(\frac{\partial w}{\partial x}\right)^2 + \frac{\partial w}{\partial x}\frac{\partial w^*}{\partial x}\right]\end{array}\right\} dA \end{aligned} \tag{6}$$

Herein, k_1 and k_2 are the stiffness coefficients of Winkler elastic foundation and the shear layer.

The corresponding Euler-Lagrange equation can be written as

$$\frac{\partial^2}{\partial x^2}\frac{\partial L}{\partial w_{,xx}} - \frac{\partial}{\partial x}\frac{\partial L}{\partial w_{,x}} + \frac{\partial L}{\partial w} = 0 \tag{7}$$

in which, $w_{,xx} = \dfrac{\partial^2 w}{\partial x^2}, w_{,x} = \dfrac{\partial w}{\partial x}$.

Substituting Eq. (6) into Eq. (7), one has

$$\begin{aligned} &-A_0\frac{\partial}{\partial x}\left\{\left(\left[\frac{\partial u}{\partial x} + \frac{1}{2}\left(\frac{\partial w}{\partial x}\right)^2 + \frac{\partial w}{\partial x}\frac{\partial w^*}{\partial x}\right] + N^T\right)\left(\frac{\partial w}{\partial x} + \frac{\partial w^*}{\partial x}\right)\right\} \\ &+A_2\frac{\partial^4 w}{\partial x^4} + k_1 w - k_2\frac{\partial^2 w}{\partial x^2} = 0, \\ &\frac{\partial N_x}{\partial x} = \frac{\partial}{\partial x}\left\{A_0\left[\frac{\partial u}{\partial x} + \frac{1}{2}\left(\frac{\partial w}{\partial x}\right)^2 + \frac{\partial w}{\partial x}\frac{\partial w^*}{\partial x}\right] - N^T\right\} = 0. \end{aligned} \tag{8}$$

Herein

$$[A_0, A_2] = \int_A E(1, z^2) dA. \tag{9}$$

Take the antiderivative of the second equation in Eq. (8) with respect to x for one time and once more, and we can get the following expressions, as

$$\begin{aligned} &N_x = A_0\left[\frac{\partial u}{\partial x} + \frac{1}{2}\left(\frac{\partial w}{\partial x}\right)^2 + \frac{\partial w}{\partial x}\frac{\partial w^*}{\partial x}\right] - N^T = C_1, \\ &u(x,t) = C_2 + \frac{C_1}{A_0}x + \frac{N_T}{A_0}x - \int_0^x\left[\frac{1}{2}\left(\frac{\partial w}{\partial x}\right)^2 + \frac{\partial w}{\partial x}\frac{\partial w^*}{\partial x}\right]dx. \end{aligned} \tag{10}$$

Due to u (0) =$u(L)$=0, so

$$\begin{cases} u|_{x=0} = -\int_0^x\left[\frac{1}{2}\left(\frac{\partial w}{\partial x}\right)^2 + \frac{\partial w}{\partial x}\frac{\partial w^*}{\partial x}\right]dx\Big|_{x=0} + \frac{C_1}{A_0}\times 0 \\ + \frac{N_T}{A_0}\times 0 + C_2 = C_2 = 0 \\ u|_{x=L} = \int_0^x\left[\frac{1}{2}\left(\frac{\partial w}{\partial x}\right)^2 + \frac{\partial w}{\partial x}\frac{\partial w^*}{\partial x}\right]dx\Big|_{x=L} + \frac{C_1}{A_0}\times L \\ + \frac{N_T}{A_0}\times L + C_2 = 0 \end{cases} \tag{11}$$

Then, we can obtain

$$\begin{aligned} &N_x = C_1 = \int_0^L\left[\frac{A_0}{2L}\left(\frac{\partial w}{\partial x}\right)^2 + \frac{A_0}{L}\frac{\partial w}{\partial x}\frac{\partial w^*}{\partial x}\right]dx - N_T, C_2 = 0, \\ &u(x,t) = \int_0^L\left[\frac{1}{2L}\left(\frac{\partial w}{\partial x}\right)^2 + \frac{1}{L}\frac{\partial w}{\partial x}\frac{\partial w^*}{\partial x}\right]dx \\ &-\int_0^x\left[\frac{1}{2}\left(\frac{\partial w}{\partial x}\right)^2 + \frac{\partial w}{\partial x}\frac{\partial w^*}{\partial x}\right]dx. \end{aligned} \tag{12}$$

Substituting Eq. (13) into Eq. (7), one has

$$\begin{aligned} &A_2\frac{\partial^4 w}{\partial x^4} - \left\{\int_0^L\left[\frac{A_0}{2L}\left(\frac{\partial w}{\partial x}\right)^2 + \frac{A_0}{L}\frac{\partial w}{\partial x}\frac{\partial w^*}{\partial x}\right]dx - N_T\right\} \\ &\times\left(\frac{\partial^2 w}{\partial x^2} + \frac{\partial^2 w^*}{\partial x^2}\right) + k_1 w - k_2\frac{\partial^2 w}{\partial x^2} = 0 \end{aligned} \tag{13}$$

Define the following dimensionless quantities

$$\begin{aligned} &K_1 = k_1\frac{L^4}{D\pi^4}, K_2 = k_2\frac{L^2}{D\pi^2}, \gamma_T = \frac{A_x^T L^2}{D\pi^2}, \ \gamma_0 = \frac{L^2 A_0}{\pi^2 D}, \\ &\gamma_1 = A_2\frac{1}{D}, W = \frac{w}{L}, X = \frac{\pi x}{L}, \ W^* = \frac{w^*}{L}. \end{aligned} \tag{14}$$

Substituting Eq. (14) into Eq. (13), one has

$$\begin{aligned} &-\left\{\int_0^\pi\left[\frac{\pi\gamma_0}{2}\left(\frac{\partial W}{\partial X}\right)^2 + \pi\gamma_0\frac{\partial W}{\partial X}\frac{\partial W^*}{\partial X}\right]dX - \gamma_T\Delta T\right\} \\ &\times\left(\frac{\partial^2 W}{\partial X^2} + \frac{\partial^2 W^*}{\partial X^2}\right) + \gamma_1\frac{\partial^4 W}{\partial X^4} + K_1 W - K_2\frac{\partial^2 W}{\partial X^2} = 0 \end{aligned} \tag{15}$$

3. Solving the governing equation

In the following part, we consider three different boundary conditions, including the clamped-clamped ends (C-C), simply supported ends (S-S), and one end clamped and one end simply supported (C-S). The two-step perturbation method (Shen 2013, Shen 2014) is also used to solve the whole problem. The solution satisfying the boundary conditions can be set as

$$\begin{cases} W = A_{10}^{(1)}[1-\cos(2X)], W^* = A_{11}[1-\cos(2X)], \ \text{(C-C)}; \\ W = A_{10}^{(1)}\sin(X), \ W^* = A_{11}\sin(X), \ \text{(S-S)}; \\ W = A_{10}^{(1)}\left[\cos\left(\frac{X}{2}\right) - \cos\left(\frac{3}{2}X\right)\right], \\ W^* = A_{11}\left[\cos\left(\frac{X}{2}\right) - \cos\left(\frac{3}{2}X\right)\right], \ \text{(C-S)}. \end{cases} \tag{16}$$

Substituting Eq. (16) into Eq. (15), one can obtain

$$\begin{aligned} &\mathbb{N}(X) = -16\gamma_1 A_{10}^{(1)}\cos(2X) + (\gamma_T\Delta T - \pi^2\gamma_0(A_{10}^{(1)})^2 \\ &-2\pi^2\gamma_0 A_{11}A_{10}^{(1)}) + K_1 A_{10}^{(1)}(1-\cos(2X)) \\ &-4K_2 A_{10}^{(1)}\cos(2X) = 0, \ \text{(C-C)}; \\ &\mathbb{N}(X) = (\gamma_T\Delta T - \frac{\pi^2}{4}\gamma_0(A_{10}^{(1)})^2 - \frac{\pi^2}{2}\gamma_0 A_{11}A_{10}^{(1)}) \\ &\cdot\left(A_{10}^{(1)}\sin(2X) + A_{11}\sin(2X)\right) + K_1 A_{10}^{(1)}\sin(2X) \\ &+K_2 A_{10}^{(1)}\sin(2X) + \gamma_1 A_{10}^{(1)}\sin(2X) = 0, \ \text{(S-S)}; \\ &\mathbb{N}(X) = \left(\gamma_T\Delta T - \frac{5}{8}\pi^2\gamma_0(A_{10}^{(1)})^2 + \frac{5}{4}\pi^2\gamma_0 A_{11}A_{10}^{(1)}\right) \\ &\cdot\left(\frac{1}{4}\left(A_{10}^{(1)} + A_{11}\right)\cos\left(\frac{X}{2}\right) - \frac{9}{4}\left(A_{10}^{(1)} + A_{11}\right)\cos\left(\frac{3X}{2}\right)\right) \\ &+\left(K_1 - K_2\right)A_{10}^{(1)}\left(\cos\left(\frac{X}{2}\right) - \frac{9}{4}\cos\left(\frac{3X}{2}\right)\right) \\ &+\gamma_1 A_{10}^{(1)}\left(\frac{1}{16}\cos\left(\frac{X}{2}\right) - \frac{81}{16}\cos\left(\frac{3X}{2}\right)\right) = 0, \ \text{(C-S)}. \end{aligned} \tag{17}$$

Applying Galerkin principle to Eq. (17), one can get

$$\begin{aligned} &\int_0^\pi \mathbb{N}(X)\cdot[1-\cos(2X)]dX, \ (C-C) \\ &\int_0^\pi \mathbb{N}(X)\cdot\sin(X)dX, \ (S-S) \\ &\int_0^\pi \mathbb{N}(X)\cdot\left[\cos\left(\frac{X}{2}\right) - \cos\left(\frac{3}{2}X\right)\right]dX, \ (C-S) \end{aligned} \tag{18}$$

Finally, the thermal-buckling path of the porous FG pipes with initial geometric imperfection, as

For $A_{11} \neq 0$

$$\Delta T = \begin{cases} \left(\frac{3K_1 + 4K_2 + 16\gamma_1 + 8\pi^2\gamma_0 {A_{11}}^2 - 4\gamma_T\Delta T}{8\gamma_T A_{11}}\right) \\ \times\frac{R_0}{L}\left(\frac{w_m}{R_0}\right) + \frac{3\pi^2\gamma_0}{4\gamma_T}\left(\frac{R_0}{L}\right)^2\left(\frac{w_m}{R_0}\right)^2 \\ +\frac{\pi^2\gamma_0}{8\gamma_T A_{11}}\left(\frac{R_0}{L}\right)^3\left(\frac{w_m}{R_0}\right)^3, (C-C); \\ \left(\frac{2K_1 + 2K_2 + 2\gamma_1 + \pi^2\gamma_0 {A_{11}}^2 - 2\gamma_T\Delta T}{2\gamma_T A_{11}}\right) \\ \times\frac{R_0}{L}\left(\frac{w_m}{R_0}\right) + \frac{3\pi^2\gamma_0}{4\gamma_T}\left(\frac{R_0}{L}\right)^2\left(\frac{w_m}{R_0}\right)^2 \\ +\frac{\pi^2\gamma_0}{4\gamma_T A_{11}}\left(\frac{R_0}{L}\right)^3\left(\frac{w_m}{R_0}\right)^3, (S-S); \\ \left(\frac{32K_1 + 40K_2 + 82\gamma_1 + 50\pi^2\gamma_0 {A_{11}}^2 - 40\gamma_T\Delta T}{40\gamma_T A_{11}}\right) \\ \cdot\frac{50}{77}\cdot\frac{R_0}{L}\cdot\left(\frac{w_m}{R_0}\right) + \frac{15\pi^2\gamma_0}{8\gamma_T}\left(\frac{50}{77}\right)^2\left(\frac{R_0}{L}\right)^2\left(\frac{w_m}{R_0}\right)^2 \\ +\frac{5\pi^2\gamma_0}{8\gamma_T A_{11}}\left(\frac{50}{77}\right)^3\left(\frac{R_0}{L}\right)^3\left(\frac{w_m}{R_0}\right)^3, \ (C-S). \end{cases} \tag{19}$$

Table 1 Temperature-dependent coefficients, from Reddy (2000), Zhang and She (2022)

Materials	Proprieties	P_0	P_{-1}	P_1	P_2	P_3	P(TID)
Si_3N_4	E(Pa)	348.43e+9	0.0	-3.070e-4	2.160e-7	-8.964e-11	322.27e+9
	α (1/K)	5.8723e-6	0.0	9.095e-4	0.0	0.0	7.4746e-6
SUS304	E(Pa)	201.04e+9	0.0	3.079e-4	-6.543e-7	0.0	207.79e+9
	α (1/K)	12.33e-6	0.0	8.086e-4	0.0	0.0	15.32e-6

For $A_{11}=0$

$$\Delta T=\begin{cases}\Delta T_{cr}+\dfrac{\pi^2\gamma_0}{\gamma_T}\left(\dfrac{R_0}{L}\right)^2\left(\dfrac{w_m}{R_0}\right)^2, \ (C-C);\\ \Delta T_{cr}+\dfrac{\pi^2\gamma_0}{4\gamma_T}\left(\dfrac{R_0}{L}\right)^2\left(\dfrac{w_m}{R_0}\right)^2, \ (S-S);\\ \Delta T_{cr}+\dfrac{5\pi^2\gamma_0}{8\gamma_T}\left(\dfrac{50}{77}\right)^2\left(\dfrac{R_0}{L}\right)^2\left(\dfrac{w_m}{R_0}\right)^2, \ (C-S).\end{cases} \tag{20}$$

in which

$$\Delta T_{cr}=\begin{cases}\dfrac{3K_1+4K_2+16\gamma_1}{4\gamma_T},(C-C);\\ \dfrac{K_1+K_2+\gamma_1}{\gamma_T}, \ (S-S);\\ \dfrac{16K_1+20K_2+41\gamma_1}{20\gamma_T}, \ (C-S).\end{cases} \tag{21}$$

and

$$A_{10}^{(1)}=\begin{cases}\dfrac{R_0}{2L}\left(\dfrac{w_m}{R_0}\right), \ (C-C);\\ \dfrac{R_0}{L}\left(\dfrac{w_m}{R_0}\right), \ (S-S);\\ \dfrac{50}{77}\dfrac{R_0}{L}\left(\dfrac{w_m}{R_0}\right), \ (C-S).\end{cases} \tag{22}$$

4. Numerical analyses

The materials used in the following numerical analysis are shown in Table 1. To ensure the correctness of this paper, we conducted comparative analysis with the existing results. In Tables 2 and 3, we considered the FG pipes with simply supports and clamped supports at both ends. During calculation, $K_1=K_2=0$, $A_{11}=0$, $\beta=0$. Through comparison, we can see that the results of this paper are basically consistent with existing literature based on higher order shear deformation theory (Fu *et al.* 2015, She *et al.* 2017a), thus verifying the correctness of this study.

In Fig. 2, we study the influence of initial geometric imperfection on the post-thermal-buckling response of pipe structures. As seen, the abscissa represents deflection and the ordinate represents temperature load. It can be seen that the pipe structures with and without initial geometric imperfection show significantly different deflection-load response relationships. That is, the initial geometric imperfection has a significant impact on the thermal post-buckling problem. Bifurcation buckling exists for pipes with the initial geometric imperfection. On the contrary, there is no bifurcation buckling for pipes without initial geometric imperfection, especially when the deflection is relatively small. However, with the increase of deflection, the thermal post-buckling response with initial geometric imperfection and the thermal post-buckling response without defects tend to be the same.

In Fig. 3, we study the influence of functional graded index N on the thermal post-buckling response of the pipe structures. Similarly, it can be seen that, first, the pipe structures with and without initial geometric imperfection show different deflection-load response relations, that is to say, the initial geometric imperfection has significant impacts on the thermal post-buckling problems. Bifurcation buckling exists for pipes with initial geometric defects. On

Table 2 Comparisons of ΔT_{cr} (in K) for FG pipes with two clamped ends

N	Present	She *et al.* (2017a)
0	844.294	816.356
1	692.516	675.204
2	643.212	626.906
3	613.823	598.374
4	593.328	579.154
5	579.021	565.298
6	568.773	554.832
7	559.106	546.645
8	553.015	540.069
9	549.535	534.669
10	544.121	530.155

Table 3 Comparisons of ΔT_{cr} (in K) for FG pipes with simply supported ends

L/R_0	Present	Fu *et al.* (2015)
15	888.216	853.293
20	555.325	542.027
25	380.745	377.243
30	272.452	277.344
35	208.352	212.049
40	160.274	167.077
45	130.166	134.842
50	102.001	110.989

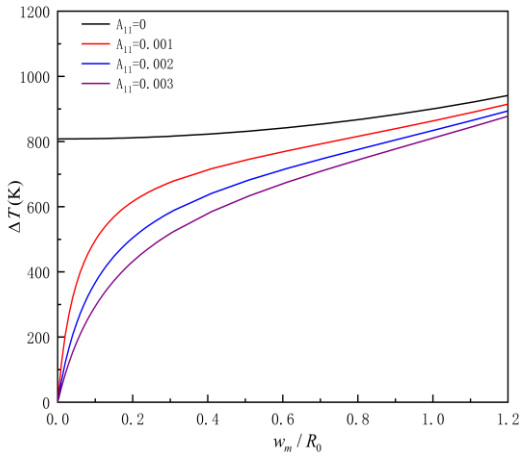

(a)

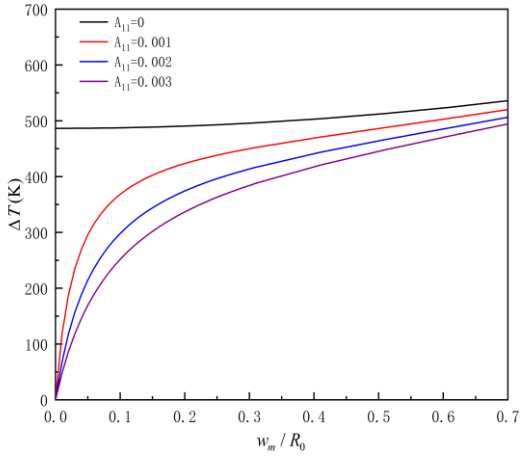

(b)

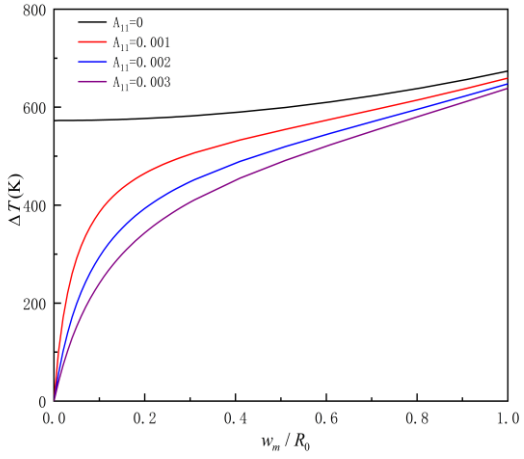

(c)

Fig. 2 Effect of initial geometric imperfection on the thermal post-buckling response for the Si_3N_4/SUS304 pipes at $L/R_0 = 40$, $R_0 = 2R_i$, $K_1 = 2$, $K_2 = 0$, $N = 1$, $\beta = 0.1$; (a) C-C, (b) S-S and (c)C-S

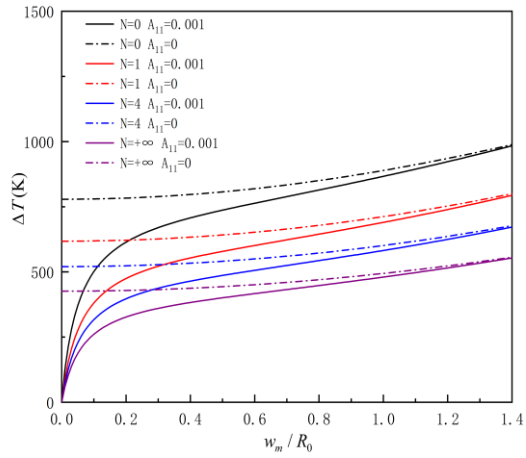

(a)

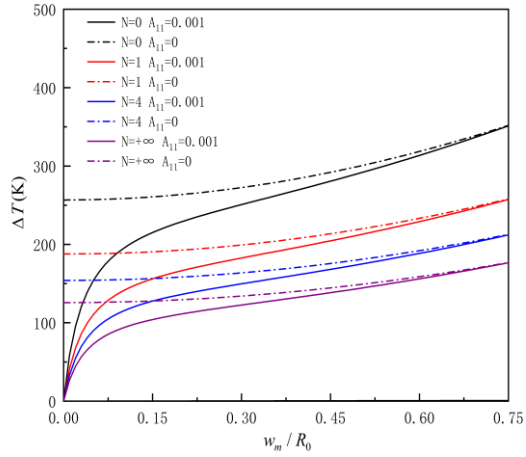

(b)

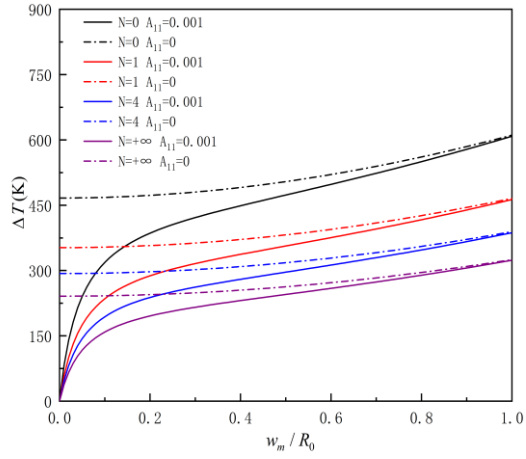

(c)

Fig. 3 Effect of functionally graded index on the thermal post-buckling response for the Si_3N_4/SUS304 pipes at $L/R_0 = 40$, $R_0 = 2R_i$, $K_1 = 2$, $K_2 = 0$, $N = 1$, $\beta = 0.1$; (a) C-C; (b) S-S and (c) C-S

the contrary, there is no bifurcation buckling for pipes without initial geometric imperfection, especially when the initial geometric imperfection is relatively small. Secondly, with the increase of functional graded index N, the critical buckling load decreases and the response curves of thermal post-buckling is at a lower position. This is because with the increase of N, the content of ceramics decreases and the corresponding content of metal increases, so the stiffness of the whole pipe structure also decreases (She *et al.* 2017a, 2017b). Thirdly, the boundary conditions have particularly significant effects on the thermal post-buckling responses. The pipe with clamped-clamped has higher thermal-buckling load and thermal post-buckling response, while the simply supported pipe has the smallest thermal-buckling

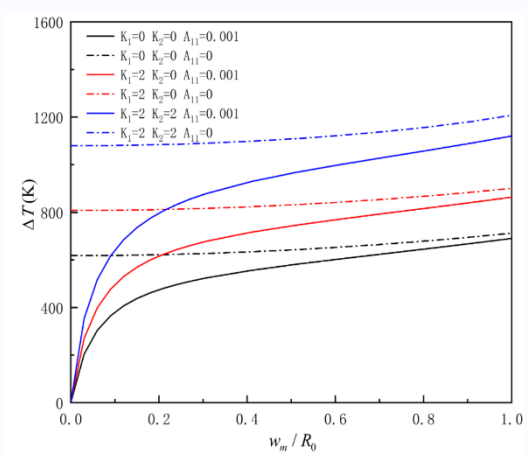

(a)

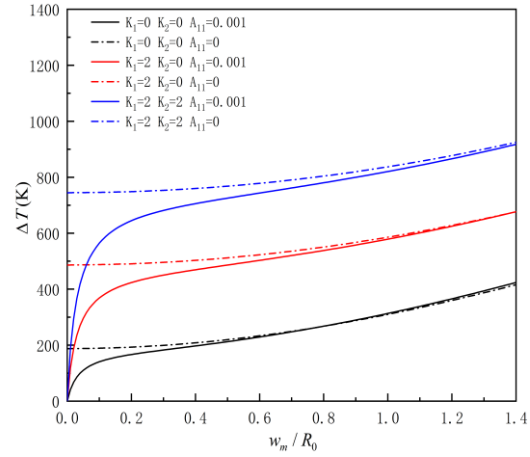

(b)

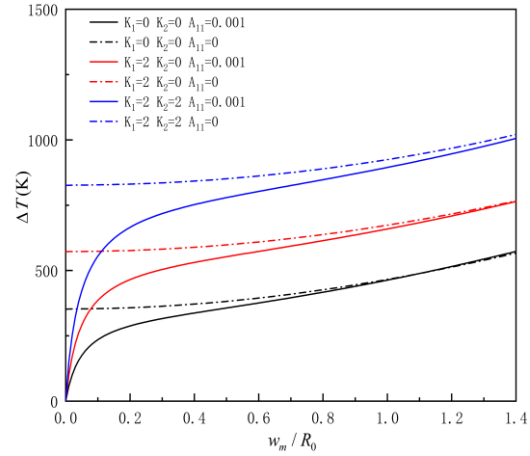

(c)

Fig. 4 Effect of the elastic foundation stiffness on the thermal post-buckling response for the Si_3N_4/SUS304 pipes at L/R_0 = 40, R_0 = 2R_i, N= 1, β =0.1; (a) C-C, (b) S-S and (c) C-S

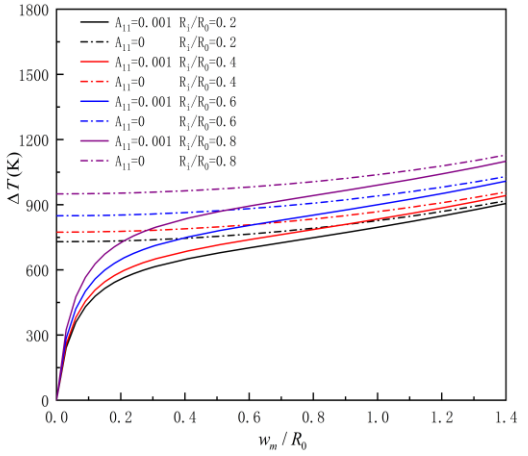

(a)

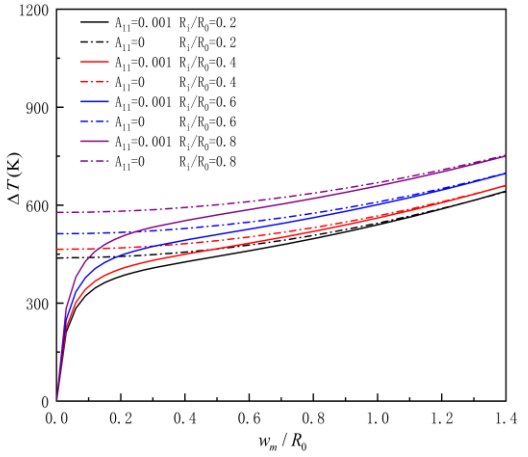

(b)

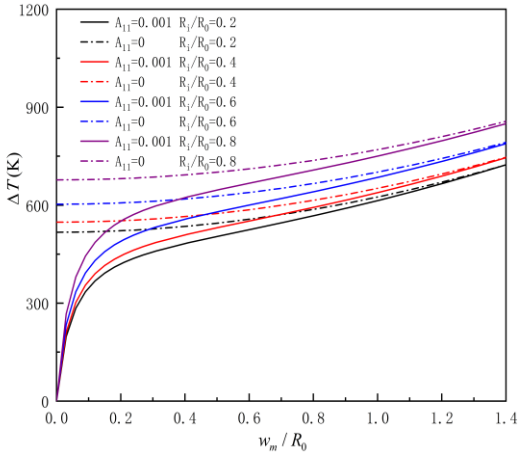

(c)

Fig. 5 Effect of the thickness of pipe on the thermal post-buckling load–deflection curves of Si3N4/SUS303 pipes for L/R_0 = 40, N= 1, K_1= 2, K_2=0, β =0.1; (a) C-C, (b) S-S and (c)C-S

load and thermal post-buckling response. The C-S pipe is in between the two cases.

In Fig. 4, the influence of elastic foundation on thermal post-buckling response of pipe structures is studied. It can be seen that the elastic stiffness can significantly improve the thermal post-buckling load and thermal post-buckling strength. This is because the elastic foundation increases the stiffness of the system. Therefore, the spring coefficient plays an important role in predicting the buckling response of FG pipes under thermal environment.

In Fig. 5, the influence of thickness on the thermal post-buckling response of pipe structures is studied. As seen, the thickness of pipe can significantly change the buckling load and the thermal post-buckling strength. The thinner the

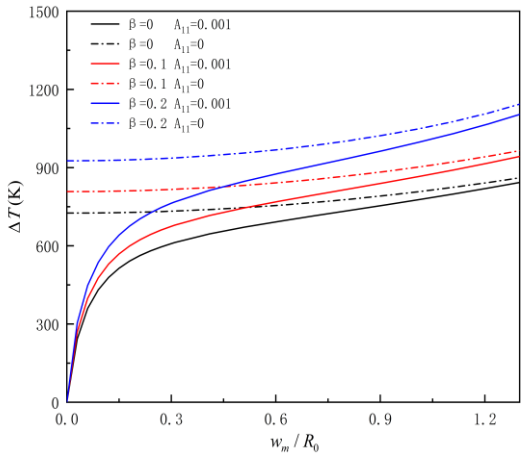

Fig. 6 Effect of the porosity on the thermal post-buckling load–deflection curves of Si3N4/SUS303 pipes for L/R_0 = 40, R_0=2R_i, K_1=2, K_2=0, N= 1, (a) C-C, (b) S-S and (c)S-C

thickness of the pipe is, the greater the critical thermal-buckling loads and the thermal-buckling strength, which is due to the excellent mechanical properties of thin-walled structures.

In Fig. 6, the effect of porosity coefficient on the thermal post-buckling response of FG pipe is illustrated. As seen, the porosity coefficient can significantly change the critical buckling load and the thermal post-buckling strength. As seen, the larger the porosity coefficient is, the greater the thermal buckling load and the thermal buckling strength, which indicates that the strength and stiffness of the FG pipes are further decreased owing to the increasing porosity coefficient.

5. Conclusions

In this paper, the thermal post-buckling of functionally gradient pipes is investigated. Considering the initial geometric imperfection and geometric nonlinearity, the Euler-Lagrange equation is used to derive the nonlinear governing equation of the pipe. Considering three different boundary conditions, the thermal post-buckling response is solved by the two-step perturbation method. Through numerical analyses, we found that:

Firstly, the pipes with and without initial geometric imperfection show significantly different deflection-load response relationships. For the pipes without initial geometric imperfection, bifurcation buckling exists. On the contrary, there is no bifurcation buckling for pipes with initial geometric imperfection.

Second, with the increase of functionally graded index N, the critical buckling load decreases, and so does the thermal post-buckling strength.

Thirdly, the boundary conditions have a particularly significant effect on the thermal post-buckling response. The clamped pipe has higher critical thermal buckling load and thermal post-buckling response, while the simply supported pipe has the smallest thermal buckling load and thermal post-buckling response.

Fourth, the elastic stiffness can significantly improve thermal post-buckling load and thermal post-buckling strength. This is because the elastic stiffness can increase the stiffness of the system.

Fifth, the thinner the thickness of the pipe, the greater the load and strength of thermal post-buckling, because thin-walled structures have excellent mechanical properties.

Sixth, Porosity can significantly change the load and strength of thermal post-buckling. The larger the porosity, the greater the thermal buckling load and the thermal buckling strength.

Acknowledgments

This work is supported by the talent introduction project of Chongqing University (02090011044159), and Fundamental Research Funds for the Central Universities (2022CDJXY-005), and the project of new technology and equipment of intelligent manufacturing (02090025020040).

References

Alnujaie, A., Akba, E.D., Eltaher, M. and Assie, A. (2021). "Forced vibration of a functionally graded porous beam resting on viscoelastic foundation", *Geomech. Eng.*, **24**(1). http://doi.org/10.12989/gae.2021.24.1.091.

Akba, E.D., Bashiri, A.H., Assie, A.E. and Eltaher, M.A. (2021),

"Dynamic analysis of thick beams with functionally graded porous layers and viscoelastic support", *J. Vib. Control*, **27**(13-14), 1644-1655. http://doi.org/10.1177/1077546320947302.

Akgöz, B. and Civalek, O. (2017), "Effects of thermal and shear deformation on vibration response of functionally graded thick composite microbeams", *Compos. Part B: Eng.*, **129**, 77-87. https://doi.org/10.1016/j.compositesb.2017.07.024.

Amar, L.H.H., Kaci, A., Yeghnem, R. and Tounsi, A. (2018), "A new four-unknown refined theory based on modified couplestress theory for size-dependent bending and vibration analysis of functionally graded micro-plate", *Steel Compos. Struct.*, **26**(1), 89-102. https://doi.org/10.12989/scs.2018.26.1.089.

Asiri, S.A., Akba, E.D. and Eltaher, M. (2020), "Damped dynamic responses of a layered functionally graded thick beam under a pulse load", *Struct. Eng. Mech.*, **75**(6), 713-722. http://doi.org/10.12989/sem.2020.75.6.713.

Attia, M.A. and Mohamed, S.A. (2020a), "Thermal vibration characteristics of pre/post-buckled bi-directional functionally graded tapered microbeams based on modified couple stress Reddy beam theory", *Eng. Comput.*, https://doi.org/10.1007/s00366-020-01188-4.

Attia, M.A. and Mohamed, S.A. (2020b), "Nonlinear thermal buckling and postbuckling analysis of bidirectional functionally graded tapered microbeams based on Reddy beam theory", *Eng. Comput.*, https://doi.org/10.1007/s00366-020-01080-1.

Babaei, H. (2021a), "Thermoelastic buckling and post-buckling behavior of temperature-dependent nanocomposite pipes reinforced with CNTs", Eur. Phys. J. Plus, **136**(10). http://doi.org/10.1140/epjp/s13360-021-01992-x.

Babaei, H.(2021b), "Large deflection analysis of fg-cnt reinforced composite pipes under thermal-mechanical coupling loading", *Structures*, **34**, 886-900. http://doi.org/10.1016/j.istruc.2021.07.091.

Babaei, H. (2021c), "Nonlinear analysis of size-dependent frequencies in porous fg curved nanotubes based on nonlocal strain gradient theory", *Eng. With Comput.*, http://doi.org/10.1007/s00366-021-01317-7.

Babaei, H. and Eslami, M. (2021a). "Nonlinear analysis of thermal-mechanical coupling bending of clamped fg porous curved micro-tubes", *J. Therm. Stresses*, 1-24. http://doi.org/10.1080/01495739.2020.1870417.

Babaei, H. and Eslami, M. (2021b), "Thermally induced nonlinear stability and imperfection sensitivity of temperature- and size-dependent fg porous micro-tubes", *Int. J. Mech. Mater. Design*, 1-21. http://doi.org/10.1007/s10999-021-09531-3.

Dehrouyeh-Semnani, A.M., Dehdashti, E., Yazdi, M. and Nikkhah-Bahrami, M. (2019), "Nonlinear thermo-resonant behavior of fluid-conveying FG pipes", *Int. J. Eng. Sci.*, **144**, 103141. https://doi.org/10.1016/j.ijengsci.2019.103141.

Ding, H.X. and She, G.L. (2021), "A higher-order beam model for the snap-buckling analysis of FG pipes conveying fluid", *Struct. Eng. Mech.*, **80**(1), 63-72. https://doi.org/10.12989/sem.2021.80.1.063.

Ebrahimi, F. and Farazmandnia, N. (2018), "Vibration analysis of functionally graded carbon nanotube-reinforced composite sandwich beams in thermal environment", *Adv. Aircraft Sp. Sci.*, **5**(1), 107-128. https://doi.org/10.12989/aas.2018.5.1.107.

Emam, S. (2016), "Buckling and postbuckling of composite beams in hygrothermal environments", *Compos. Struct.*, **152**, 665-675. http://doi.org/10.1016/j.compstruct.2016.05.029.

Fu, Y., Zhong, J., Shao, X. and Chen, Y. (2015), "Thermal postbuckling analysis of functionally graded tubes based on a refined beam model", *Int. J. Mech. Sci.*, **96**, 58-64. http://doi.org/10.1016/j.ijmecsci.2015.03.019.

Ghandourah, E.E., Eltaher, M.A., Ahmed, H.M., Attia, M.A. and Abdraboh, A.M. (2021), "Free vibration of porous fg nonlocal modified couple nanobeams via a modified porosity model", *Adv. Nano Res.*, **11**(4). http://doi.org/10.12989/anr.2021.11.4.405.

Golmakani, M.E., Malikan, M. and Pour, S.G. (2021), "Bending analysis of functionally graded nanoplates based on a higher-order shear deformation theory using dynamic relaxation method", *Continuum Mech. Thermodynam.*, https://doi.org/10.1007/s00161-021-00995-4.

Hadji, L., Meziane, M. and Safa, A. (2018), "A new quasi-3d higher shear deformation theory for vibration of functionally graded carbon nanotube-reinforced composite beams resting on elastic foundation", *Struct. Eng. Mech.*, **66**(6), 771-781. https://doi.org/10.12989/sem.2018.66.6.771.

Hendi, A., Eltaher, M.A., Mohamed, S.A. and Attia, M. (2022), "Nonlinear thermal vibration of pre/post-buckled two-dimensional FGM tapered microbeams based on a higher order shear deformation theory", *Steel Compos. Struct.*, **41**(6), 787-802. https://doi.org/10.12989/scs.2022.41.6.787.

Lu, L., She, G.L. and Guo, X. (2021), "Size-dependent postbuckling analysis of graphene reinforced composite microtubes with geometrical imperfection", *Int. J. Mech. Sci.*, **199**, 106428. https://doi.org/10.1016/j.ijmecsci.2021.106428.

Mohamed, N., Mohamed, S. and Eltaher, M. (2020), "Buckling and post-buckling behaviors of higher order carbon nanotubes using energy-equivalent model", *Eng. Comput.*, **37**(4). http://doi.org/10.1007/s00366-020-00976-2.

Mohamed, N., Mohamed, S.A. and Eltaher, M.A. (2022), "Nonlinear static stability of imperfect bio-inspired helicoidal composite beams", *Mathematics*, **10**(7). http://doi.org/10,7.10.3390/math10071084.

Pinnola, F.P., Vaccaro, M.S., Barretta, R., Francesco, M. and Ruta, G. (2022), "Elasticity problems of beams on reaction-driven nonlocal foundation", *Arch. Appl. Mech.*, 1-31. http://doi.org/10.1007/s00419-022-02161-x.

Reddy, J.N. (2000), "Analysis of functionally graded plates", *Int. J. Numer. Method. Eng.*, **47**(1-3), 663-684. http://doi.org/10.1002/(SICI)10970207(20000110/30)47:1/3<663::AID-NME787>3.0.CO;2-8.

She, G.L. (2021), "Guided wave propagation of porous functionally graded plates: The effect of thermal loadings", *J. Therm. Stresses*, **44**(10), 1289-1305. https://doi.org/10.1080/01495739.2021.1974323.

She, G.L., Ding, H.X. and Zhang, Y.W. (2022), "Wave propagation in a FG circular plate via the physical neutral surface concept", *Struct. Eng. Mech.*, **82**(2), 225-232. https://doi.org/10.12989/sem.2022.82.2.225.

She, G.L., Liu, H.B. and Karami, B. (2021), "Resonance analysis of composite curved microbeams reinforced with graphenenanoplatelets", *Thin Wall. Struct.*, **160**, 107407. https://doi.org/10.1016/j.tws.2020.107407.

She, G.L., Yuan, F.G. and Ren, Y.R. (2017a), "Nonlinear analysis of bending, thermal buckling and post-buckling for functionally graded tubes by using a refined beam theory", *Compos. Struct.*, **165**, 74-82. https://doi.org/10.1016/j.compstruct.2017.01.013.

She, G.L., Yuan, F.G., Ren, Y.R. and Xiao, W.S. (2017b), "On buckling and postbuckling behavior of nanotubes", *Int. J. Eng. Sci.*, **121**, 130-142. https://doi.org/10.1016/j.ijengsci.2017.09.005.

Shen, H.S. (2013), A Two-Step Perturbation Method in Nonlinear Analysis of Beams, Plates and Shells, John Wiley & Sons Inc., Singapore.

Shen, H.S. (2014), "Postbuckling of FGM cylindrical panels resting on elastic foundations subjected to axial compression under heat conduction", *Int. J. Mech. Sci.*, **89**, 453-461. https://doi.org/10.1061/(ASCE)AS.1943-5525.0000439.

Zenkour, A.M. and Radwan, A.F. (2019), "Bending response of FG plates resting on elastic foundations in hygro thermal

environment with porosities", *Compos. Struct*., **213**, 133-143. https://doi.org/10.1016/j.compstruct.2019.01.065.

Zhao, J.L., Chen, X., She, G.L., Jing, Y., Bai, R.Q., Yi, J., Pu, H.Y., and Luo, J. (2022), "Vibration characteristics of functionally graded carbon nanotube-reinforced composite double-beams in thermal environments", *Steel Compos. Struct*., **43**(6), 797-808. https://doi.org/10.12989/scs.2022.43.6.797.

Zhang, Y.Y., Wang, Y.X., Zhang, X., Shen, H.M. and She, G.L. (2021), "On snap-buckling of FG-CNTR curved nanobeams considering surface effects", *Steel Compos. Struct*., **38**(3), 293-304. https://doi.org/10.12989/scs.2021.38.3.293.

Zhang,Y.W. and She,G.L. (2022), "Wave propagation and vibration of FG pipes conveying hot fluid", *Steel Compos. Struct.*, 42(3), 397-405. https://doi.org/10.12989/scs.2022.42.3.397.

CC